ARTICLES

Photophysics of 3-Substituted Benzanthrones: Substituent and Solvent Control of Intersystem Crossing

Peter Kapusta,[†] Oldřich Machalický,[§] Radim Hrdina,[§] Miloš Nepraš,[§] Matthew B. Zimmt,*[,‡] and Vlastimil Fidler*[,†,‡]

Department of Physical Electronics, Czech Technical University in Prague, 180 00 Czech Republic, Department of Chemistry, Brown University, Providence, Rhode Island 02912, and Department of Organic Technology, University of Pardubice, Pardubice, 532 10 Czech Republic

Received: June 6, 2003; In Final Form: September 9, 2003

The solvent dependence of absorption and fluorescence spectra, fluorescence lifetimes (τ_{Fl}), and quantum yields (q_{Fl}) of various 3-substituted benzanthrone derivatives have been investigated. A consistent correlation between fluorescence quantum yield and emitting state energy has been found that holds for all 6 derivatives in 11 solvents. The experimental data together with the results of semiempirical quantum chemical calculations indicate that the main quenching channel of the fluorescent $S_1(\pi,\pi^*)$ excited state is intersystem crossing to an upper (n,π^*) triplet state, T_N. The rate constant and efficiency of intersystem crossing between these two states are strongly influenced by the substituent and by the solvent polarity, as both modulate the singlet state energy and the S_1-T_N energy gap. The rate constant of direct $S_1 \rightarrow T_1$ intersystem crossing is small in most systems but appears to increase with a decrease in the energy of the S_1 state.

Introduction

There is growing interest in application of 3-substituted benzanthrone derivatives as structural probes in chemistry and biology. Yang et al. used 3-methoxybenzanthrone as a solvatochromic fluorescence probe of DNA intercalation.[1] Grabchev et al. synthesized benzanthrone derivatives bearing azomethine and oxy groups at the C-3 position and studied them using absorption and fluorescence spectroscopy in liquid,[2] as well as in crystalline media.[3] Their work provides a phenomenological description of the C-3 substituent's influence on the dye absorption and fluorescence features based on an intramolecular electron donor−acceptor interaction between the electron donating C-3 substituent and the electron accepting carbonyl group.

Molecular structure control of intramolecular electronic energy transfer is another area of recent interest, inspired by biology and molecular optoelectronics.[4] In some cases, through-bond spacer-mediated intramolecular singlet−singlet electronic energy transfer is much faster than the corresponding through-space contribution—see, for example, refs 4 and 5. In such a case, donor and/or acceptor photophysics plays a more complex role than that within a system in which Förster energy transfer is dominant. Recently we found[6] that electronic energy transfer in a bichromophoric compound containing aminopyrene as a donor, triazine as a spacer, and aminobenzanthrone as an acceptor takes place with a rate coefficient higher than 3×10^{12} s^{-1}, much faster then expected. The possible role of a specific aminobenzanthrone chromophore photophysics in such a system is not fully understood.

In a previous paper, we reported the synthesis, absorption, and fluorescence spectra of several 3-substituted benzanthrone compounds with special attention devoted to the reactive *N*-(1,3,5-triazinyl)-3-aminobenzanthrone derivatives.[7] See Figure 1A for the structures, abbreviations, and numbering conventions used here. On the basis of PPP-MO theory, we explained the influence of various N-substituents on the absorption spectra in terms of the electron donating ability of the amino nitrogen.[7] The explanation proved to be sufficiently general that this simple model also described the behavior of the chemically distinct 3-*N*-acetylamino- and 3-methoxybenzanthrone analogues. In that work we reported remarkable differences in the fluorescence quantum yields of the various derivatives, particularly in low polarity solvents.[7]

In an effort to understand the origin of the unusual photophysics of the 3-substituted benzanthrone derivatives, a broader range of photophysical data were analyzed in conjunction with more sophisticated quantum chemical calculations. In this paper we present data on absorption and fluorescence spectral maxima, fluorescence quantum yields, and lifetimes for 6 benzanthrone derivatives in 11 different solvents. Temperature-dependent fluorescence lifetime data and emission anisotropy data are presented for selected compounds. The experimental data are accompanied by results of electronic ground- and excited-state calculations using Hartree−Fock, AM1, and INDO/S methods. The results provide a coherent picture of solvation effects on the excited-state energy and its influence on intersystem crossing rate constants in the 3-substituted benzanthrone compounds.

Experimental Section

The syntheses of the new compounds used in this study were reported elsewhere.[7] The samples for absorption and fluores-

* Corresponding author. E-mail: Vlastimil_Fidler@Brown.Edu.
[†] Czech Technical University in Prague.
[‡] Brown University.
[§] University of Pardubice.

10.1021/jp035610a CCC: $25.00
Published on Web 10/29/2003

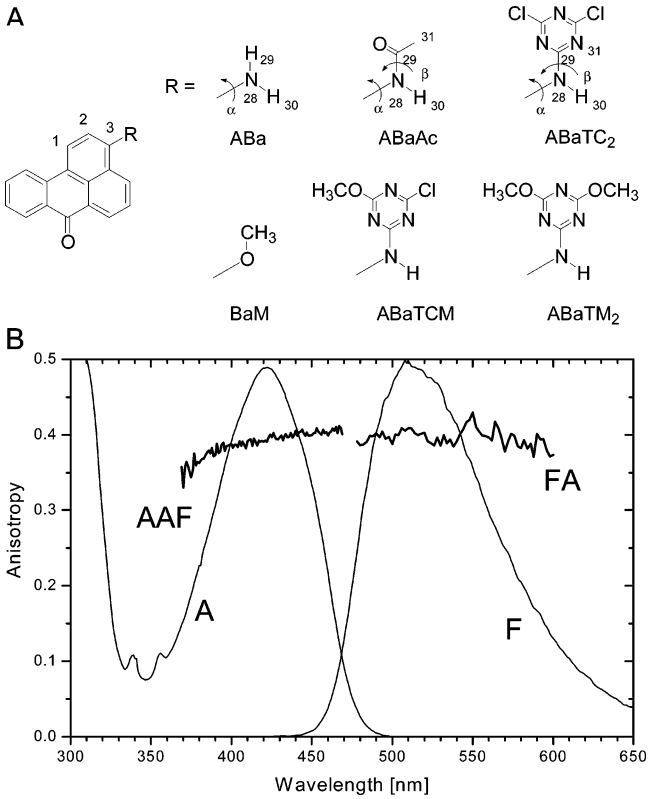

Figure 1. (A) The structures, abbreviations and numbering conventions of the compounds studied. (B) Absorption (A) and fluorescence (F) spectra of ABaAc in 2MeTHF at room temperature; absorption wavelength-dependent anisotropy of fluorescence (AAF) detected at 510 nm, and fluorescence wavelength-dependent anisotropy (FA) for 405 nm excitation in MeTHF solvent at 77 K.

cence measurements were prepared by preparative thin-layer chromatography on Silufol UV 254 plates. All solvents used were spectral or HPLC grade. All spectroscopic measurements were done at room temperature (21 °C) unless stated otherwise. Absorption spectra were measured on a Perkin-Elmer 555 spectrophotometer using solution concentrations on the order of 10^{-5} M, which yielded optical densities of nearly 0.5 at the main absorption maximum in 1 cm cuvettes. Steady-state fluorescence spectra were measured on a Hitachi Perkin-Elmer LS 5 spectrofluorimeter. The instrument provides corrected excitation spectra directly; the fluorescence emission spectra were corrected for the characteristics of the emission monochromator and the photomultiplier response. Samples used for fluorescence measurements had an optical density ≈ 0.05 at the exciting wavelength in 1 cm cuvettes. Fluorescence quantum yields were measured using quinine sulfate in 0.1 N H_2SO_4 ($q_{Fl} = 0.54$, $n_D = 1.33$) or perylene ($q_{Fl} = 0.89$ in benzene, $n_D = 1.50$) as standards.[8] Deoxygenation of the samples by bubbling with N_2 or Ar did not alter the spectra or quantum yields; thus, the reported data correspond to aerated solutions.

Steady-state fluorescence anisotropy, isotropic ns/ps fluorescence decay kinetics, and their temperature dependence were measured on an extended Edinburgh Instrument FS/FL900 steady-state/time-resolved spectrofluorimeter that utilizes time-correlated single photon counting (TCSPC) detection. The system was equipped with an IBH NanoLED-07 (405 nm ps diode laser), a NanoLED-05A (370 nm ns LED), and a nanosecond flash lamp as pulsed light sources, a Hammamatsu MCP−PMT fast detector, and an Oxford Instrument Optistat DN cryostat. The instrumental response function fwhm was <60 ps when the 405 nm diode laser was used as the excitation source. Fluorescence lifetimes were determined by iterative multiexponential reconvolution fitting.

TABLE 1: Selected Dielectric Parameters of the Solvents Used: Electric Dipole Moment in Solution ($\vec{\mu}$ [10^{-30} C·m]), Dielectric Constant (ϵ_r), and Refractive Index (n_D) at Room Temperature

solvent	abbr	$\vec{\mu}$	ϵ_r	n_D	$F(\epsilon,n)$
toluene	TOL	1.0	2.38	1.4969	0.013
chlorobenzene	CLB	5.4	5.62	1.5248	0.142
benzonitrile	CBN	13.4	25.20	1.5282	0.235
dibutyl ether	DBE	3.9	3.08	1.3992	0.096
diethyl ether	DIE	3.8	4.20	1.3524	0.162
ethyl acetate	ETA	6.1	6.02	1.3724	0.200
cyclohexanone	CHO	10.3	16.10	1.4510	0.243
acetone	ACE	9.0	20.56	1.3587	0.284
acetonitrile	ACN	11.8	35.94	1.3441	0.305
2-propanol	PRO	5.5	20.45	1.3856	0.274
methanol	MEO	5.7	32.66	1.3284	0.309

Results and Discussion

I. Spectral Data. Absorption and fluorescence maximum data in 11 solvents for BaM, ABa, and 4 of its derivatives are presented in Table 2, while Table 1 summarizes the main dielectric parameters of the solvents used. Each compound exhibits a broad, structureless absorption band centered between 20 000 and 25 000 cm^{-1} (as e.g. ABaAc in Figure 1B) with an oscillator strength $f \sim 0.4-0.7$.[9] INDO/S calculations (Table 3) predict S_1 to be an nπ^* state with a very weak $S_0 \rightarrow S_1$ transition near 24 000 cm^{-1} and predict S_2 to be a $\pi\pi^*$ state with an intense $S_0 \rightarrow S_2$ transition ($f \sim 0.6$) near 30000 cm^{-1}. The observed, structureless absorption bands are assigned as $\pi\pi^*$ transitions on the basis of oscillator strength considerations. The compounds' fluorescence spectra (as in Figure 1B) are approximate mirror images of the intense absorption band, suggesting that the state formed upon excitation into this band is the originating state for the fluorescence. Three lines of evidence support this assertion. First, steady-state absorption and fluorescence anisotropy values in frozen MTHF are nearly 0.4 (Figure 1B). Second, radiative rate constants determined from the quantum yield and lifetime data (vide infra) agree with values calculated from the absorption spectra.[9] Finally, INDO/S values of the ground-state and $\pi\pi^*$-state dipole moment vectors are sufficient to reproduce the solvent dependence of both the absorption and emission maxima (vide infra). Although INDO/S calculations (Table 3) assign S_1 as an nπ^* state, the experimental data indicate $\pi\pi^*$ character for S_1. The calculations do not account for solvation effects. $\pi\pi^*$ excited states are more polarizable than nπ^* excited states.[10] Additionally, the benzanthrone $\pi\pi^*$ states' dipole moments are larger than the nπ^* states' dipoles (Table 3). Solvation may lower the $\pi\pi^*$ states' energy to the extent that they lie below the corresponding nπ^* states and may be responsible for the divergent conclusions reached by theory and experiment regarding the nature of S_1.

The absorption maxima of the $\pi\pi^*$ transition in the six molecules exhibit varied solvent dependences (Figure 2). The band maxima of ABa and BaM exhibit significant bathochromic shifts with increasing polarity in aprotic solvents. The bathochromic shift observed for $ABaTC_2$ and ABaTCM in aprotic solvents is half as steep as that for ABa and BaM, whereas the band maxima of $ABaTM_2$ and ABaAc exhibit no significant solvent dependence. Ab initio and INDO/S calculations predict ground-state dipole moments of ~5 D in ABa and BaM. INDO/S calculations indicate that the dipole moments of the vertically formed $\pi\pi^*$ states of ABa and BaM are nearly parallel to and double the magnitudes of the molecules' ground-state

TABLE 2: Absorption and Fluorescence Maximum Positions ($\tilde{\nu}_{abs}$ and $\tilde{\nu}_{Fl}$, Respectively), Emitting-State Energy (E_{S1}), Fluorescence Quantum Yield (q_{Fl}), and Fluorescence Lifetime (τ_{Fl}) of the Studied Benzanthrone Derivatives in 11 Solvents

	$\tilde{\nu}_{abs}$ [cm^{-1}]	$\tilde{\nu}_{Fl}$ [cm^{-1}]	E_{S1} [cm^{-1}]	q_{Fl}	τ_{Fl} [ns]	$\tilde{\nu}_{abs}$ [cm^{-1}]	$\tilde{\nu}_{Fl}$ [cm^{-1}]	E_{S1} [cm^{-1}]	q_{Fl}	τ_{Fl} [ns]
			ABaTC$_2$					BaM		
TOL	24 330	19 630	21 980	0.09	0.9	23 980	20 000	21 990	0.10	1.4
DBE	24 940	20 160	22 550	0.02	0.5	24 270	20 530	22 400	0.01	0.6
CLB	24 390	19 420	21 905	0.23	2.0	23 640	19 690	21 665	0.41	6.0
DIE	24 940	19 960	22 450	0.04	0.7	24 150	20 080	22 115	0.05	0.9
ETA	24 810	19 530	22 170	0.14	1.6	23 920	19 760	21 840	0.23	4.1
CBN	24 390	19 230	21 810	0.43	6.0	23 360	19 230	21 295	0.69	14.1
CHO	24 390	19 230	21 810	0.32	3.4	23 700	19 230	21 465	0.57	7.8
PRO	24 280	17 950	21 115	0.46	7.7	22 990	18 480	20 735	0.54	12.7
ACE	24 690	19 190	21 940	0.36	4.5	23 750	19 230	21 490	0.56	10.5
ACN	24 810	18 980	21 895	0.43	6.6	23 470	18 980	21 225	0.62	13.2
MEO	24 390	17 540	20 965	0.44	7.6	23 200	17 830	20 515	0.45	12.6
			ABaTCM					ABaAc		
TOL	23 810	19 300	21 555	0.27	2.8	23 870	19 380	21 625	0.21	2.8
DBE	24 750	19 720	22 235	0.05	0.9	23 810	19 720	21 765	0.07	1.9
CLB	23 920	19 050	21 485	0.50	5.4	23 810	19 230	21 520	0.51	5.9
DIE	24 690	19 450	22 070	0.12	1.6	23 920	19 300	21 610	0.19	2.6
ETA	24 330	19 230	21 780	0.34	3.9	23 870	19 230	21 550	0.46	6.6
CBN	24 040	19 010	21 525	0.58	7.8	23 590	18 940	21 265	0.62	9.8
CHO	24 100	19 080	21 590	0.51	6.3	23 530	18 980	21 255	0.64	8.3
PRO	23 980	17 540	20 760	0.50	8.0	23 980	17 610	20 795	0.49	9.3
ACE	24 390	18 980	21 685	0.54	7.7	23 810	19 010	21 410	0.62	9.7
ACN	24 570	18 590	21 580	0.52	8.4	24 100	18 520	21 310	0.59	10.3
MEO	24 100	17 300	20 700	0.33	7.7	24 330	17 450	20 890	0.33	8.6
			ABaTM$_2$					ABa		
TOL	23 420	19 160	21 290	0.56	5.6	21 690	17 570	19 630	0.30	9.2
DBE	23 700	19 380	21 540	0.22	3.7	21 320	17 540	19 430	0.34	9.2
CLB	23 200	18 980	21 090	0.66	7.4	21 550	17 270	19 410	0.25	8.6
DIE	23 980	19 230	21 605	0.39	4.9	20 960	17 090	19 025	0.26	9.5
ETA	23 870	19 120	21 495	0.58	7.3	20 700	16 890	18 795	0.21	7.1
CBN	23 200	18 660	20 930	0.64	7.0	20 790	16 390	18 590	0.14	7.5
CHO	23 640	18 800	21 220	0.67	7.4	20 450	16 390	18 420	0.15	7.8
PRO	23 700	17 360	20 530	0.38	7.7	19 340	15 040	17 190	0.03	2.0
ACE	23 870	18 730	21 300	0.66	8.5	20 320	16 390	18 355	0.11	6.9
ACN	24 160	18 050	21 105	0.59	9.2	20 410	15 970	18 190	0.10	5.9
MEO	23 810	17 040	20 425	0.30	7.4	19 450	14 990	17 220	0.02	1.5

dipole moments (Table 3). Equilibrium solvent polarization induced by the ground-state dipole of ABa or BaM interacts more favorably with the larger excited-state dipole moment. Consequently, the vertical, $\pi\pi^*$ excited state is solvated to a greater extent than the ground state and the absorption maximum shifts bathochromically upon increasing the solvent polarity.[11]

The ground-state dipole moments of the amino-substituted derivatives ABaAc and ABaTC$_2$ are 4.3 and 3.3 D. The dihedral angles involving the amine nitrogen (see Figure 1A) indicate more extensive conjugation to the acyl or triazinyl substitutent ($\beta \equiv C_3-N_{28}-C_{29}-(C_{31},N_{31}) \sim 179°$) than to the benzanthrone group ($\alpha \equiv C_2-C_3-N_{28}-C_{29} \sim 28-58°$). The calculated dipole moments of these molecules' vertically formed $\pi\pi^*$ states (7.1 and 4.7 D, respectively) are 40−65% larger than the ground-state moments but are displaced by 35° from the direction of the ground state dipole. Solvent polarization induced by the ground state is not aligned to effectively solvate the larger excited-state dipole; consequently, the solvent induced shifts of these molecules' absorption maxima are small.

The fluorescence maxima of all six compounds red shift with increasing solvent polarity. The variation with solvent is largest for ABa and BaM. The solvent dependence of the emission maxima arises from different charge distributions within S_0 and S_1 at the excited state equilibrium geometry. The structure of the benzanthrone core probably changes little upon excitation. However, a change in electron distribution upon excitation may alter the extent of conjugation with the nitrogen (oxygen) substituents, change the dihedral angles involving the substituents (i.e., the angles α and β), and generate different dipole moments in the vertically formed and relaxed excited-state geometries. To probe whether structural relaxation within S_1 significantly alters the excited-state dipole moment, the absorption and emission maxima in nonprotic solvents[12] were analyzed using the McRae−Bayliss solvation model.[11] Ground ($\vec{\mu}_0$) and excited state ($\vec{\mu}_1$) dipole moment vectors in the S_0 equilibrium geometry were calculated using the INDO/S method. The solvent dependence of the absorption maxima was fit to eq 1 using the calculated dipole vectors and adjusting two parameters, the vacuum value of the absorption maximum, $\bar{\nu}_{abs}^{vac}$, and the radius, *a*, of the dielectric cavity containing the solute (see Table 3 for the fitting parameters).

$$\bar{\nu}_{abs} = \bar{\nu}_{abs}^{vac} - 4\pi\frac{\vec{\mu}_0(\vec{\mu}_1 - \vec{\mu}_0)}{\hbar c a^3}\left[\left(\frac{\epsilon_s - 1}{2\epsilon_s + 1}\right) - \left(\frac{n^2 - 1}{2n^2 + 1}\right)\right] - 4\pi\frac{(\vec{\mu}_1^{\,2} - \vec{\mu}_0^{\,2})}{\hbar c a^3}\left(\frac{n^2 - 1}{2n^2 + 1}\right) \quad (1)$$

Once the cavity radius was determined from the absorption analysis, the solvent dependence of the emission maximum was fit to eq 2, varying *only* the vacuum value of the emission maximum, $\bar{\nu}_{em}^{vac}$ (Table 3).

$$\bar{\nu}_{em} = \bar{\nu}_{em}^{vac} - 4\pi\frac{\vec{\mu}_1(\vec{\mu}_0 - \vec{\mu}_1)}{\hbar c a^3}\left[\left(\frac{\epsilon_s - 1}{2\epsilon_s + 1}\right) - \left(\frac{n^2 - 1}{2n^2 + 1}\right)\right] - 4\pi\frac{(\vec{\mu}_0^{\,2} - \vec{\mu}_1^{\,2})}{\hbar c a^3}\left(\frac{n^2 - 1}{2n^2 + 1}\right) \quad (2)$$

TABLE 3: Transition Type, Energies, Dipole Moments, Angles, and Oscillator Strengths Calculated with the INDO/S Method and Fitting Parameters[f] for the McRae−Bayliss Solvation Model

ABa

state	transition[a] $S_0 \rightarrow S_N$	energy($S_0 \rightarrow S_N$) [cm^{-1}]	$\mu(S_N)$ [D]	angle[b] (deg)	$f(S_0 \rightarrow S_N)$[c]	state	energy (cm^{-1})
S_0		0	5.0			T_1[e]	14 250
S_1	$n \rightarrow \pi^*$	24 200	1.9	38	0.00	T_2[e]	20 970
S_2	$\pi \rightarrow \pi^*$	29 300	9.4	11	0.55	T_3[d]	21 460

	fit parameters[f]	$\bar{\nu}_{abs}^{vac}$	$\bar{\nu}_{em}^{vac}$	*a* [Å]
	$\pi \rightarrow \pi^*$	22 900	19 510	4.2

BaM

state	transition[a] $S_0 \rightarrow S_N$	energy($S_0 \rightarrow S_N$) [cm^{-1}]	$\mu(S_N)$ [D]	angle[b] (deg)	$f(S_0 \rightarrow S_N)$[c]	state	energy (cm^{-1})
S_0		0	5.8			T_1[e]	16 390
S_1	$n \rightarrow \pi^*$	24 820	2.6	9	0.00	T_2[d]	22 200
S_2	$\pi \rightarrow \pi^*$	29 380	10.7	7	0.55	T_3[e]	22 450

	fit parameters[f]	$\bar{\nu}_{abs}^{vac}$	$\bar{\nu}_{em}^{vac}$	*a* [Å]
	$\pi \rightarrow \pi^*$	26 390	22 770	4.4

ABaAc

state	transition[a] $S_0 \rightarrow S_N$	energy($S_0 \rightarrow S_N$) [cm^{-1}]	$\mu(S_N)$ [D]	angle[b] (deg)	$f(S_0 \rightarrow S_N)$[c]	state	energy (cm^{-1})
S_0		0	4.3			T_1[e]	14 300
S_1	$n \rightarrow \pi^*$	24 240	3.7	54	0.00	T_2[e]	21 000
S_2	$\pi \rightarrow \pi^*$	29 310	7.1	36	0.57	T_3[d]	21 490

	fit parameters[f]	$\bar{\nu}_{abs}^{vac}$	$\bar{\nu}_{em}^{vac}$	*a* [Å]
	$\pi \rightarrow \pi^*$	24 880	20 850	4.1

$ABaTCl_2$

state	transition[a] $S_0 \rightarrow S_N$	energy($S_0 \rightarrow S_N$) [cm^{-1}]	$\mu(S_N)$ [D]	angle[b] (deg)	$f(S_0 \rightarrow S_N)$[c]	state	energy (cm^{-1})
S_0		0	3.3			T_1[e]	14 710
S_1	$n \rightarrow \pi^*$	24 060	5.1	46	0.00	T_2[e]	21 240
S_2	$\pi \rightarrow \pi^*$	30 250	4.7	37	0.64	T_3[d]	21 310

	fit parameters[f]	$\bar{\nu}_{abs}^{vac}$	$\bar{\nu}_{em}^{vac}$	*a* [Å]
	$\pi \rightarrow \pi^*$	26 640	22 730	2.4

[a] Principal orbitals involved in this transition. [b] Angle between the S_0 and S_N state dipole moments. [c] Oscillator strength. [d] $^3n\pi^*$ state. [e] $^3\pi\pi^*$ state. [f] See text and Figure 3 for an explanation of the fitting parameters.

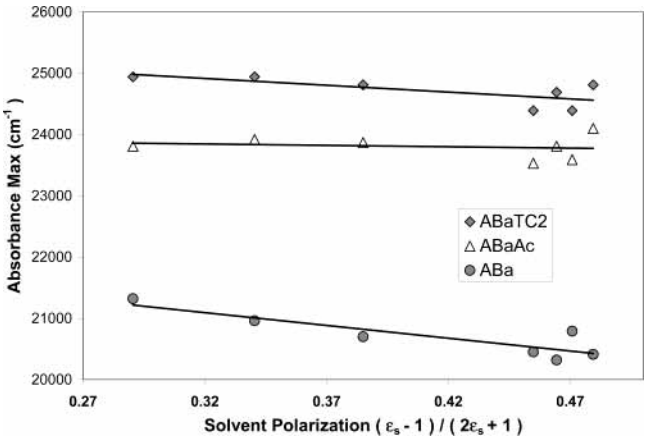

Figure 2. Solvent dependence of the absorption maxima for $ABaTC_2$, ABaAc, and ABa. The continuum polarization function $(\epsilon_s - 1)/(2\epsilon_s + 1)$ is the abscissa. The lines are linear fits to the indicated points. Data from alcohol and weakly dipolar aromatic solvents are not included.

Figure 3 displays the calculated spectral maxima versus the experimental maxima in seven solvents for BaM, ABa, ABaAc, and $ABaTCl_2$.[13] For each of the four molecules, use of the INDO/S dipole moment vectors and a state-independent radius reasonably reproduces the solvent dependence of both the absorption and emission data.[14] This result demonstrates that any structural reorganization within the S_1 excited state does not significantly alter the charge distribution or the effective size of the molecules in these solvents. The vacuum Stokes shift,[15] $\bar{\nu}_{abs}^{vac} - \bar{\nu}_{em}^{vac}$, is relatively constant for the four molecules, 3700 ± 300 cm^{-1}. The cavity radii determined for BaM and ABa are physically reasonable.[16] From simple size considerations,[16] it is surprising that the best fit cavity radius for ABaAc is *smaller* than those of BaM and ABa. For $ABaTC_2$, the deviation between the molecule's size and the best fit cavity radius, 2.4 Å, is particularly striking. The ground-state geometry of the aminobenzanthrone derivatives maximizes conjugation of the 3-nitrogen lone pair with the substituent, not with the benzanthrone. This reduces electron donation into, and the dipole moment of, the benzanthrone group. It also provides the substituent with a significant dipole moment that, in part, opposes the benzanthrone dipole. The presence of two independent dipole moment sources within $ABaTC_2$ and ABaAc likely precludes a simple, physical interpretation of the cavity radius in the solvation model. Despite its small value, the cavity radius determined from the $ABaTC_2$ absorption data accurately predicts the solvent dependence of the emission maximum. This indicates that the vertical and relaxed excited-state geometries of $ABaTC_2$ have similar dipole moments.

The compounds' fluorescence quantum yields, q_{Fl}, vary substantially among the 11 solvents. With the exception of ABa,

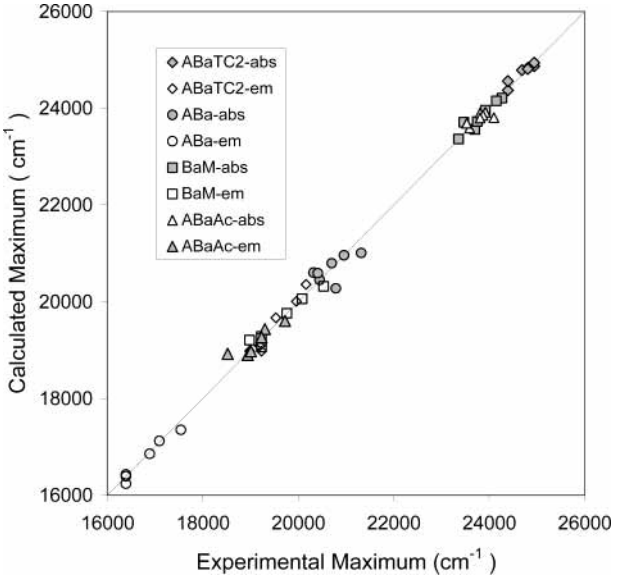

Figure 3. Comparison of best fit and experimental absorption (shaded) and emission (unshaded) maxima for $ABaTC_2$ (diamonds), ABa (circles), BaM (squares), and ABaAc (triangles) in the dipolar aprotic solvents. The straight line indicates a perfect correspondence. The dipole moments, relative orientations, and fit parameters are listed in Table 3.

the quantum yields in the aromatic solvents increase with increasing polarity (dielectric constant). In the nonaromatic, aprotic solvents, the fluorescence quantum yields of $ABaTC_2$ and BaM increase with increasing polarity, while those of ABaTCM, $ABaTM_2$, and ABaAc increase, plateau, and then decrease with increasing polarity. For ABa, the fluorescence quantum yield decreases with increasing solvent polarity. These variations arise from the solvent dependence of the nonradiative rate constants[17] (vide infra).

II. Kinetic Data. Time-resolved fluorescence decays from all six compounds are fit adequately using single-exponential functions.[18] The radiative and nonradiative rate constants are determined from the fluorescence quantum yield and fluorescence lifetime, τ, measurements using eq 3.

$$k_{\mathrm{rad}} = \frac{q_{\mathrm{Fl}}}{\tau} \qquad k_{\mathrm{nonrad}} = \frac{1 - q_{\mathrm{Fl}}}{\tau} \tag{3}$$

The radiative rate constants exhibit moderate solvent dependence, varying from 1×10^7 to 4×10^7 s^{-1} for ABa, from 4×10^7 to 12×10^7 s^{-1} for the substituted aminobenzanthrone derivatives, and from 2×10^7 to 7×10^7 s^{-1} for BaM. Solvent effects on the nonradiative rate constants vary widely; from a factor of 5 for $ABaTM_2$ to a factor of 75 for BaM. For five of the compounds, the nonradiative rate constant is largest in butyl ether and smallest in one of the polar solvents.[19] The quantum yield and nonradiative rate constants exhibit striking dependences (Figure 4) on the emitting state energy, E_{S1}, defined as the average of the absorption and emission band maxima.[20] With the exception of the case of ABa, the quantum yields are largest for $E_{00} \sim 21\,200$ cm^{-1}. Higher and lower E_{S1} values are attended by smaller quantum yields and larger nonradiative rate constants. Although ABa does not attain $E_{S1} \sim 21\,000$ cm^{-1}, its quantum yield and nonradiative rate constant exhibit energy dependences comparable to those of the other molecules for data points with E_{S1} below 21 000 cm^{-1}.

The energy dependence of q_{Fl} and k_{nonrad} may be explained in terms of two parallel intersystem crossing channels starting from the S_1 $^1\pi\pi^*$ state (Figure 5).[21] Normally, $\pi\pi^*$ configurations exhibit large singlet−triplet energy gaps, $\Delta E(\mathrm{S-T})$.[22] Thus, the lowest energy triplet state, T_1, has a $^3\pi\pi^*$ configuration with an energy substantially below that of S_1. INDO/S calculations (Table 3) confirm this.[23] The large energy gap between the T_1 and S_1 states, in conjunction with generally small spin−orbit coupling matrix elements for $^1\pi\pi^* \rightarrow {}^3\pi\pi^*$ transitions,[24] should produce small direct $S_1(^1\pi\pi^*) \rightarrow T_1(^3\pi\pi^*)$ intersystem crossing rate constants. This intersystem crossing channel should exhibit a weak dependence on S_1 energy. The second intersystem crossing channel involves higher energy $T_N(^3n\pi^*)$ states. INDO/S calculations predict that the singlet $n\pi^*$ state lies approximately 24 500 cm^{-1} above S_0. Small $\Delta E(\mathrm{S-T})$ values for $n\pi^*$ configurations[22] predict the presence of a triplet $n\pi^*$ (T_N) somewhat below the S_2 $n\pi^*$ state which should make the T_N state proximate to S_1. INDO/S calculations place the $^3n\pi^*$ state between 21 000 and 22 500 cm^{-1} (Table 3). $^1\pi\pi^* \rightarrow {}^3n\pi^*$ spin−orbit coupling matrix elements are significant;[24] thus, the energetic proximity of S_1 to T_N provides an active $S_1(^1\pi\pi^*) \rightarrow T_N(^3n\pi^*)$ intersystem crossing channel. Provided T_N is above S_1, this intersystem crossing channel will exhibit a significant activation energy. Solvents of different polarities will alter the S_1 state energy, modulate the S_1-T_N energy gap, and change the activation barrier and rate constant of the $S_1(^1\pi\pi^*) \rightarrow T_N(^3n\pi^*)$ intersystem crossing channel.[25] In systems where S_1 lies much lower in energy than the $^3n\pi^*$ state, only the $S_1 \rightarrow T_1$ intersystem crossing channel should be active. This two-channel intersystem crossing explanation is consistent with the variation of k_{nonrad} for E_{S1} between 19 000 and 22 500 cm^{-1} (Figure 4B). The increase of k_{nonrad} in ABa as E_{S1} drops below

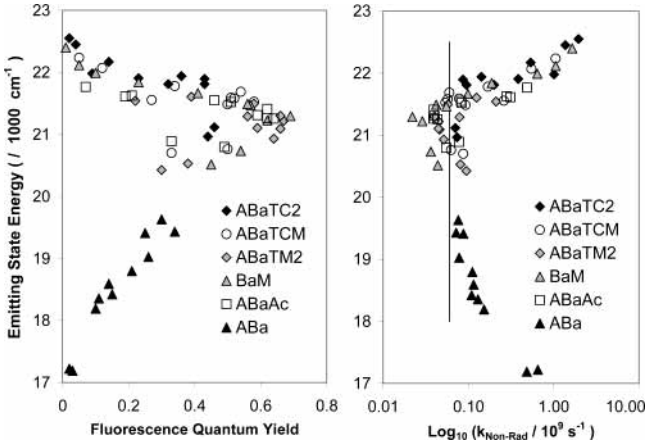

Figure 4. (A) Correlation between the emitting state energy (E_{S1}) and the fluorescence quantum yield. (B) Correlation between the emitting state energy (E_{S1}) and the log of the nonradiative rate constant. The vertical line in panel B marks the mean radiative rate constant of the six compounds.

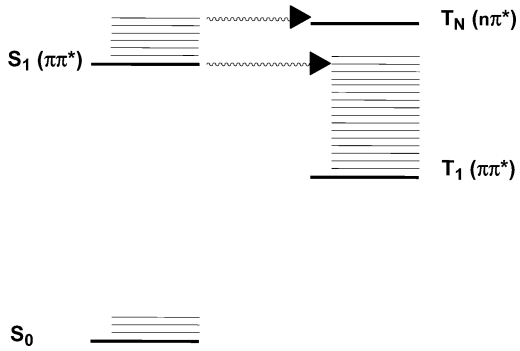

Figure 5. Energy diagram for the proposed two channel intersystem crossing model.

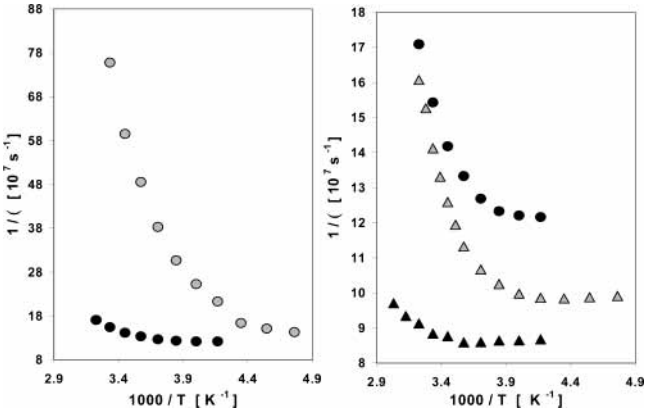

Figure 6. Temperature dependence of the S_1 decay rate constant for $ABaTC_2$ (circles) and ABaAc (triangles) in ethyl acetate (gray) and acetonitrile (black).

18 500 cm^{-1} indicates an increase of the $S_1 \rightarrow T_1$ intersystem crossing rate constant.

The photophysical model proposed for the benzanthrone derivatives predicts certain temperature dependence characteristics of the decay rate constant. Intersystem crossing via the $S_1(^1\pi\pi^*) \rightarrow T_N(^3n\pi^*)$ channel should be an activated process, with a barrier that is largest in the most polar solvents.[26] By contrast, intersystem crossing via the $S_1(^1\pi\pi^*) \rightarrow T_1(^3\pi\pi^*)$ channel should not be activated and may even exhibit a weak, negative temperature dependence.[27] Contributions from both channels, and from a weakly temperature-dependent radiative rate constant, should produce a biphasic temperature dependence of the decay rate constant. To test these predictions, the temperature dependence of the decay rate constant was determined for $ABaTC_2$ in ethyl acetate ($E_{S1}^{295K} = 22\ 170\ cm^{-1}$) and acetonitrile ($E_{S1}^{295K} = 21\ 895\ cm^{-1}$) and for ABaAc in ethyl acetate ($E_{S1}^{295K} = 21\ 550\ cm^{-1}$) and acetonitrile ($E_{S1}^{295K} = 21\ 310\ cm^{-1}$). In each of these systems (Figure 6), the excited-state decay rate constant exhibits an activated behavior at higher temperatures and a plateau at the lowest temperatures. The plateau values of the rate constants are 40−80% larger than the room-temperature radiative rate constants for each compound in the corresponding solvent. The differences ($(3-6) \times 10^7\ s^{-1}$) provide estimates of the direct $S_1(^1\pi\pi^*) \rightarrow T_1(^3\pi\pi^*)$ intersystem crossing rate constant for these compounds.

The increase of the rate constant at higher temperatures unambiguously establishes the existence of an activated decay channel for the benzanthrone molecules. Given the qualitative observation of decreased fluorescence quantum yield with increasing temperature, this activated process is attributed to the $S_1(^1\pi\pi^*) \rightarrow T_N(^3n\pi^*)$ intersystem crossing channel. The temperature dependence of this intersystem crossing channel varies considerably depending on the compound and the solvent. For $ABaTC_2$ in ethyl acetate, the total decay rate constant increases five hundred percent ($60 \times 10^7\ s^{-1}$) from the plateau value (at 200 K) to the rate constant at 300 K. In acetonitrile, the rate increases only fifty percent between the plateau value and the room temperture rate. The rate increases for ABaAc are less dramatic: 60% from the plateau region to 310 K in ethyl acetate; 15% from the plateau to 330 K in acetonitrile.

The barrier heights for $S_1(^1\pi\pi^*) \rightarrow T_N(^3n\pi^*)$ may be compared qualitatively by noting the temperatures at which the activated $S_1(^1\pi\pi^*) \rightarrow T_N(^3n\pi^*)$ intersystem crossing process is fast enough to increase the total rate above the plateau value. These temperatures are ~230 K for $ABaTC_2$ in ethyl acetate, 280 K for $ABaTC_2$ in acetonitrile, 270 K for ABaAc in ethyl acetate, and 310 K for ABaAc in acetonitrile. This qualitative analysis indicates a larger activation barrier for ABaAc than for $ABaTC_2$ in a given solvent, which is consistent with the lower S_1 energy of ABaAc. The analysis also indicates a larger activation barrier in acetonitrile than in ethyl acetate for both molecules. Again, this trend is consistent with the lower S_1 energy for either molecule in acetonitrile. Overall, the temperature dependence of the decay rate constants is consistent with the qualitative predictions of the two-channel intersystem crossing model.

Conclusion

The steady-state and time-resolved emission data from 3-substituted benzanthrone derivatives in a wide range of solvents exhibit a remarkably consistent dependence on singlet-state energy. Emission quantum yields are largest and nonradiative rate constants are smallest for solvent/substrate combinations that engender a lowest excited singlet state energy near 21 300 cm^{-1}. The emission data are explained using a photophysical model with two intersystem crossing channels that have widely different dependences on singlet-state energy. For most of the derivatives at room temperature, the dominant nonradiative decay pathway is the activated $S_1(\pi\pi^*) \rightarrow T_N(n\pi^*)$ intersystem crossing channel. The rate of this intersystem crossing process increases with S_1 state energy. Nonradiative decay by way of the activationless $S_1(\pi\pi^*) \rightarrow T_1(\pi\pi^*)$ intersystem crossing channel becomes increasingly important as the energy of the S_1 state decreases. The temperature dependence of the decay rate constant is consistent with the two-channel model: the nonradiative rate constant is temperature independent at low temperatures but exhibits activated character at higher temperatures. The distinct solvent dependences of the absorption and emission maxima for the benzanthrone derivatives are readily explained in terms of the orientation and magnitudes of the state-dependent dipole moments. These results establish a clearer picture of the spectroscopy and photophysics of 3-substituted benzanthrone derivatives that will be of use for studies employing related derivatives as functioning components in energy-transfer arrays and for the development of new fluorescent structural probes in biology.

Acknowledgment. The initial stage of this project was supported by research grant 202/98/0566 of GACR; the later stage was supported by grant J04/98:210000022 of the Ministry of Education, Czech Republic. M.B.Z. acknowledges financial support from the National Science Foundation (CHE-0108945). Valuable assistance from Professor Robert Cave (Harvey Mudd College) and Dr. Marshall Newton (Brookhaven National Laboratory) is gratefully acknowledged.

Supporting Information Available: One figure displaying the experimental and calculated absorption and emission maxima for ABa, ABaAc, $ABaTC_2$, and BaM versus the continuum polarization function $(\epsilon_s - 1)/(2\epsilon_s + 1)$. This material is available free of charge via the Internet at http://pubs.acs.org.

References and Notes

(1) Yang, X.; Liu, W.-H.; Jin, W.-J.; Shen, G.-L.; Yu, R.-Q. *Spectrochim. Acta A* **1999**, *55*, 2719.

(2) Grabchev, I.; Moneva, I.; Wolarz, E.; Bauman, D.; Stouyanov, S. *Z. Naturforsch.* **2001**, *56a*, 291.

(3) Grabchev, I.; Moneva, I.; Wolarz, E.; Bauman, D. *Dyes Pigm.* **2003**, *58*, 1.

(4) (a) Speiser, S.; Schael, F. *J. Mol. Liq.* **2000**, *86*, 25. (b) Ramsteiner, I. B.; Hartshuch, A.; Port, H. *Chem. Phys. Lett.* **2001**, *343*, 83. (c)

Schweitzer, G.; Grondheid, R.; Jordens, S.; Lor, M.; De Belder, G.; Weil, T.; Reuther, E.; Müllen, K.; De Schryver, F. C. *J. Phys. Chem. A* **2003**, *107*, 3199.

(5) Nishimura, Y.; Yasuda, A.; Speiser, S.; Yamazaki, I. *Chem. Phys. Lett.* **2000**, *323*, 117 and references therein.

(6) Fidler, V.; Kapusta, K.; Nepraš, M.; Schroeder, J.; Rubtsov, I. V.; Yoshihara, K. *Z. Phys. Chem.* **2002**, *216*, 589.

(7) Nepraš, M.; Machalický, O.; Šeps, M.; Hrdina, R.; Kapusta, P.; Fidler, V. *Dyes Pigm.* **1997**, *35*, 31.

(8) Birks, J. B. *Fluorescence quantum yield measurements*; National Bureau of Standards, Special Publication No. 466; Washington, DC, 1977. Birks, J. B.; Dyson, D. J. *Proc. R. Soc* **1963**, *A275*, 135.

(9) Birks, J. B. *Photophysics of Aromatic Molecules*; Wiley-Interscience: London, 1970; pp 51 and 87.

(10) (a) Liptay, W. *Excited States* **1974**, *1*, 129. (b) Mathies, R.; Albrecht, A. C. *J. Chem. Phys.* **1974**, *60*, 2500. (c) Barker, J. W.; Noe, L. J. *J. Chem. Phys.* **1972**, *58*, 3035.

(11) (a) Bayliss, N. S.; McRae, E. G. *J. Phys. Chem.* **1954**, *58*, 1002. (b) McRae, E. G. *J. Phys. Chem.* **1957**, *61*, 562.

(12) This analysis excludes toluene and chlorobenzene, as the quadrupole moments in these solvents contribute significantly to solvation. This effect is not reproduced by the continuum model. For dipole solvation in nondipolar solvents analysis, see: (a) Reynolds, L.; Gardecki, J. A.; Frankland, S. J. V.; Horng, M. L.; Maroncelli, M. *J. Phys. Chem.* **1996**, *100*, 10337. (b) Matyushov, D. V.; Voth, G. A. *J. Chem. Phys.* **1999**, *111*, 3630.

(13) The Supporting Information (Figure S1) includes plots of the experimental and best fit (McRae−Bayliss model) absorption and emission maximum data for ABa, BaM, ABaAc, and ABaTCl2 versus the static dielectric constant reaction field. The use of the latter parameter for the *x*-axis is arbitrary.

(14) The solvent dependence of the emission spectral maxima is larger than the solvent dependence of the absorption spectral maxima. Using the latter to determine the cavity radius provides a more stringent test of the constancy of the dipole moment in the vertical and relaxed excited-state geometries.

(15) In principle, the vacuum Stokes shift reflects differences in the equilibrium geometries (bond lengths, angles, torsional angles, and vibrational frequencies) of the ground and excited states (i.e., the internal reorganization energy). The numerical difference is approximately twice the internal reorganization energy.

(16) (a) It is common to use 40% of a planar chromophore's long axis length as its cavity radius.[16b] This yields 4.9 Å for ABaAc, 4.5 Å for BaM, and 4.0 Å for ABa. (b) Lippert, E. *Z. Electrochem.* **1957**, *61*, 962.

(17) Medvedev, E. S.; Osherov, V. I. *Radiationless Transitions in Polyatomic Molecules*; Springer-Verlag: New York, 1995.

(18) In a few cases, better fits are obtained by adding <2% of a fast decaying component.

(19) The solvent dependence of the nonradiative rate constants for ABa is different. The rate constant is smallest in dibutyl ether and largest in methanol.

(20) Although this definition of the emitting state energy is arbitrary and not exactly equal to the zero−zero energy of the transition (E_{00}), similar correlations to those in Figure 4 are produced using a variety of definitions of the emitting state energy.

(21) (a) Hamanoue, K.; Nakayama, T.; Ikenaga, K.; Ibuki, K. *J. Photochem. Photobiol. A* **1993**, *74*, 147. (b) Bruni, M. C.; Ponterini, G.; Scoponi, M. *J. Phys. Chem.* **1989**, *93*, 678.

(22) Turro, N. J. *Modern Molecular Photochemistry*; Benjamin-Cummings: Menlo Park, CA, 1978; p 186.

(23) In benzanthrone, T_1 lies 16 000 cm^{-1} above S_0. Morgan, D. D.; Warshawsky, D.; Atkinson, T. *Photochem. Photobiol.* **1977**, *25*, 31.

(24) (a) El-Sayed, M. A. *J. Chem. Phys.* **1963**, *38*, 2834. (b) El-Sayed, M. A. *Annu. Rev. Phys. Chem.* **1975**, *26*, 235.

(25) Lewitzka, F.; Loehmannsroeben, H. G. *Z. Phys. Chem. (Muenchen)* **1986**, *150*, 69.

(26) Werner, T. C.; Lyon, D. B. *J. Photochem.* **1982**, *18*, 355.

(27) (a) van der Burgt, M. J.; Jansen, L. M. G.; Huizer, A. H.; Varma, C. A. G. O. *Chem. Phys.* **1995**, *201*, 525. (b) Freed, K. F.; Jortner, J. *J. Chem. Phys.* **1970**, *52*, 6272. (c) Englman, R.; Jortner, J. *Mol. Phys.* **1970**, *18*, 145.